Journal of Applied Electrochemistry (2006) 36:369–374
DOI 10.1007/s10800-005-9079-6

Determining the atomic hydrogen surface coverage on iron and nickel electrodes under water treatment conditions

JIANKANG WANG and JAMES FARRELL*
Department of Chemical and Environmental Engineering, University of Arizona, Tucson, Arizona, 85721, USA
*(*author for correspondence, tel.: +520-621-2465, fax: +520-621-6048, e-mail: farrellj@engr.arizona.edu)*

Received 20 June 2005; accepted in revised form 26 September 2005

Key words: atomic hydrogen, hydrogen evolution, iron electrode, nickel catalyst, reductive dechlorination, zerovalent iron

Abstract

Reductive methods for removing, detoxifying, or inactivating contaminants in water often involve reactions with atomic hydrogen produced from water reduction. Knowledge of how the solution pH value and electrode potential affect the concentration of atomic hydrogen on the reactive surface will be useful for evaluating possible reaction mechanisms and in optimizing treatment schemes. Presently, there are no simple methods for determining the atomic hydrogen surface coverage on the base metals that are typically used as cathodes or sacrificial reactants in water treatment operations. This research develops and evaluates an iterative, coulometric method for determining the fractional atomic hydrogen surface coverage (θ_H) on iron and nickel electrodes under water treatment conditions. The method is applicable at pH values and potentials where proton discharge is the rate-limiting step for the hydrogen evolution reaction (HER), and is valid under conditions where the metals are covered by oxide layers that lower the apparent electron transfer coefficients by up to 40% as compared to oxide-free conditions at low pH values. The method is also able to determine the exchange current density and the rate constants for the Volmer discharge and Tafel recombination steps of the HER.

1. Introduction

Electrochemical reduction is becoming increasingly utilized for removing a wide variety of organic and inorganic compounds from contaminated waters. Inorganic compounds such as Cu^{2+} [1], UO_2^{2+} [2], TcO_4^- [3], and CrO_4^{2-} [4, 5], have been removed from water via reduction to less soluble oxidation states, while compounds such as NO_3^- and NO_2^- have been removed by reduction to volatile products such as N_2 or NH_3 [6–8]. Electrochemical reduction of organic contaminants is normally directed at detoxifying the compounds or making them susceptible to biodegradation. The most common applications of electrochemical reduction of organic contaminants include: dehalogenation of chlorinated and/or fluorinated solvents [9, 10], decoloration of wastewaters from dye baths [11, 12], dechlorination of polychlorinated biphenyls [13, 14], and inactivation of nitroaromatic compounds, such as trinitrotoluene and RDX [15, 16].

A wide variety of reductive treatment schemes have been employed, most commonly involving reduction at metal [17], graphite [18], glassy carbon [19], or diamond film electrodes [1], or reduction by corroding metals, such as iron [9, 10], zinc [20], or tin [21, 22]. There is indirect evidence that the reduction of many contaminants occurs via parallel pathways that involve: (1) direct electron transfer from the cathode or the corroding metal, (2) indirect electron transfer by atomic hydrogen produced from water reduction, or (3) hydrogenolysis by atomic hydrogen adsorbed on the electrode surface [17, 23, 24]. The best evidence for the existence of parallel pathways is that reaction product distributions and the relative reaction rates for homologous compounds are dependent on the electrode material, the electrode potential, and the solution pH value.

Several lines of evidence suggest that reaction product distributions and reactivity trends among homologous compounds are influenced by the fractional atomic hydrogen surface coverage (θ_H). For example, reduction of CT at a mercury drop electrode resulted in stoichiometric production of chloroform [25], whereas reduction of CT at nickel electrodes yielded 95% methane and $<5\%$ chloroform [17, 26]. Because Hg electrodes are known to have very low levels of adsorbed atomic hydrogen [27], the different products of CT reduction on Ni and Hg electrodes may be attributed to a mechanism involving reduction by atomic hydrogen on the nickel electrode. Higher θ_H

values at lower potentials may also explain the changes in reaction product distributions for chloroalkene reduction at nickel electrodes [17]. Parallel reaction pathways involving direct electron transfer or indirect reduction by atomic hydrogen was proposed to explain changes in the relative reduction rates of trichloroethylene (TCE) and tetrachloroethylene (PCE) by corroding iron (23). Faster dechlorination of PCE vs. TCE at neutral pH was attributed to direct reduction by the iron metal, while faster TCE vs. PCE reduction at low pH values was attributed to reduction by atomic hydrogen. The greater importance of the atomic hydrogen reduction pathway at lower pH values was attributed to increasing θ_H values with decreasing pH.

Several methods have been devised for determining θ_H values on metal cathodes, including: Fourier transform infrared (FTIR) spectroscopy [28], laser desorption/mass spectrometry [29], and coulometric methods [30]. These methods have limitations that make them unsuitable for measuring atomic hydrogen surface coverages on corroding metals or metal cathodes coated with oxides, as is the case in water treatment applications. For example, the oxides coating iron and nickel cathodes at neutral pH values interfere with FTIR and laser desorption methods. Additionally, coulometric methods such as that recently proposed by Elhamid et al. [30], are limited to cases where the electron transfer coefficient for the hydrogen evolution reaction (HER) is known, as is the case for many oxide-free metal surfaces (27). Unfortunately, determination of the electron transfer coefficient under a given set of conditions requires knowledge of θ_H, as will be shown below. The objective of this research was to develop and test an iterative method for determining the electron transfer coefficient, and subsequently θ_H values, on iron and nickel electrodes under water treatment conditions. Water treatment conditions involve metal electrodes, freely corroding metals, or nickel-plated, freely corroding iron filings [31, 32] at near neutral pH values. The method is valid only for metals that have a low rate of atomic hydrogen absorption into their lattice as compared to their rate hydrogen gas evolution, as is the case for iron and nickel.

2. Model development

The HER on metal electrodes has been found to occur via a catalytic mechanism involving a proton discharge step [27]:

$$H^+ + e^- + M \xrightarrow{k_1} M - H_{ads} \quad \text{(Volmer discharge)} \tag{1}$$

an atomic hydrogen recombination step:

$$M - H_{ads} + M - H_{ads} \xrightarrow{k_2} 2M + H_2 \quad \text{(Tafel recombination)} \tag{2}$$

and/or an electrochemical desorption step:

$$M - H_{ads} + H^+ + e^- \xrightarrow{k_3} M + H_2 \quad \text{(Heyrovsky desorption)} \tag{3}$$

where M is an active site at the electrode surface, $M - H_{ads}$ is atomic hydrogen adsorbed to a catalytic site, and k_1, k_2 and k_3 are the rate constants for each reaction. Over a wide range of potential and pH values, reaction 1 is the rate-limiting step for the HER [27]. With decreasing potential, reactions 2 or 3 may become rate-limiting due to the exponential increase in the rate of reaction 1 with decreasing electrode potential. Under circumneutral pH values, reaction 3 contributes little to the rate of hydrogen evolution [23], primarily because of the low concentration of $M - H_{ads}$ species on the electrode surface. However, with decreasing pH values, increasing $M - H_{ads}$ concentrations result in an increasing contribution of reaction 3 to the rate of H_2 evolution.

The electron transfer coefficient ($\vec{\alpha}$) for a reduction reaction is defined in the Butler–Volmer equation as [33]:

$$I = i_0 A[e^{-\vec{\alpha}F(E-E_{eq})/RT} - e^{\overleftarrow{\alpha}F(E-E_{eq})/RT}] \tag{4}$$

where I is net reaction current, i_0 is the exchange current density, A is the available electroactive surface area for the reaction, F is the Faraday constant, R is the gas constant, T is the temperature, E is the electrode potential, E_{eq} is the equilibrium potential for the redox reaction, and $\vec{\alpha}$ and $\overleftarrow{\alpha}$ are the electron transfer coefficients for the reduction and oxidation reactions, respectively. The first term in brackets represents the rate of the forward reduction reaction, while the second term gives the rate of the reverse oxidation reaction. The exchange current density depends on the reactant concentrations and the nature of the electrode material. The forward transfer coefficient depends on the number of electrons transferred $\vec{\gamma}$ before the rate determining step, the number of times the rate determining step must occur [v], and the symmetry factor [β] for the reaction [27]. For an overall reaction that involves the transfer of n electrons, the forward transfer coefficient may be expressed as [27]:

$$\vec{\alpha} = \frac{\vec{\gamma}}{v} + r\beta \tag{5}$$

where $r = 0$ if the rate determining step does not involve electron transfer, otherwise $r = 1$. The β parameter is dependent on the symmetry of the potential energy surface between the transition state and the reactant and product species [27]. For a single-step electron transfer reaction, β represents the fraction of the applied overpotential that goes toward overcoming the activation energy of the reduction reaction, while $(1 - \beta)$ represents the fraction of the overpotential that goes towards increasing the activation energy for the reverse, anodic reaction [27].

Past work has shown that reaction 1 is the rate-limiting step for the HER on iron and nickel electrodes under a wide range of conditions [27, 34]. In this case, $\vec{\gamma} = 0, v = 2$ and $r = 1$, which results in $\vec{\alpha} = \beta$. Therefore, knowledge of the symmetry factor, β, is needed to calculate θ_H values as a function of the electrode potential. Although symmetry factors, and thus $\vec{\alpha}$ values, for reaction 1 have been observed to be near 0.5 for many metal electrodes under oxide-free conditions, significantly lower values have been observed on oxide-coated electrodes [26, 35].

Under conditions where reaction 1 is the rate-limiting step, the rate of reaction 1 can be expressed as [27, 30]:

$$i_c = Fk_1[H^+](1-\theta_H)\exp\left[-\frac{\vec{\alpha}F\eta}{RT}\right] \quad (6)$$

where i_c is the cathodic current density, $[H^+]$ is the proton concentration, and the overpotential (η) is given by: $\eta = (E - E_{eq})$. The rate of a bimolecular combination reaction, such as reaction 2, can be expressed as [36]:

$$i_c = k_2 F\theta_H^2 \quad (7)$$

Under steady state conditions, the rates of reactions 1 and 2 are equal. Therefore, equation 7 can be solved for θ_H and inserted into equation 6, yielding:

$$i_c \exp\left[\frac{F\vec{\alpha}\eta}{RT}\right] = i'_0\left(1 - \frac{\sqrt{i_c}}{\sqrt{Fk_2}}\right) \quad (8)$$

where $i'_0 = Fk_2[H^+]$. If the left-hand side of equation 8, which has been previously termed the charging function [30], is plotted as a function of $\sqrt{i_c}$, a straight line should result with a slope equal to $-i'_0(k_2F)^{-0.5}$ and an intercept of i'_0. However, $\vec{\alpha}$ is unknown and cannot be determined without knowing θ_H as a function of η, as indicated in equation 6. This suggests that an iterative method can be used to determine $\vec{\alpha}$, since the correct value should lead to a linear relationship between the charging function and $\sqrt{i_c}$.

3. Materials and methods

A 1.13 cm diameter nickel or iron disk (Metal Samples Co., Mumford, AL) with a nominal surface area of 1 cm^2 was used as the working electrode in all experiments. A Hg/Hg_2SO_4 electrode (EG&G, Oak Ridge, TN) was used as the reference electrode, and a 0.3 mm diameter by 4 cm long platinum wire (Aesar, Ward Hill, MA) was used as the counter electrode. The counter electrode was encased within a Nafion® (Dupont) proton permeable membrane. All experiments were performed in 10 mM $CaSO_4$ background electrolyte solutions using an EG&G model 616 rotating disk electrode in 25 ml glass cells. In experiments conducted at pH values lower than 7, H_2SO_4 was added to adjust the solution pH.

Chronoamperometry (CA) experiments were performed to measure the steady state currents for hydrogen evolution as a function of the electrode potential. The disk electrode was rotated at a speed of 100 rpm and the solutions were continuously purged with ~100 ml min^{-1} of nitrogen gas in order to eliminate oxygen reduction as a side reaction. Before all experiments, the face of the working electrode that was exposed to the solution was chemically and mechanically polished with an EG&G electrode polishing kit. The electrode was then conditioned in the solution used for each experiment at −785 mV with respect to the standard hydrogen electrode (SHE) for 3 h prior to use. All potentials are reported with respect to the SHE.

In addition to the CA experiments, Tafel scans were also performed to determine the fractional atomic hydrogen surface coverage under freely corroding conditions (θ_H^{ocp}). These experiments used the same cell and operating conditions as the CA experiments. However, after polishing, the electrodes were allowed to equilibrate with the solutions for 2 h. Tafel scans were then performed by polarizing the electrodes ±200 mV with respect to their open circuit potentials at a scan rate of 5 mV s^{-1}.

4. Results and discussion

Equation 6 suggests that an estimate of the transfer coefficient $[\vec{\alpha}']$ may be obtained from a plot of $\log(i_c)$ vs. E, as shown in Figure 1 for the iron electrode. Since this plot ignores the potential dependence of θ_H, the $\vec{\alpha}$ value calculated from the slope of Figure 1 will be smaller than the true $\vec{\alpha}$. If the $\vec{\alpha}'$ value is used to plot the charging function vs. $\sqrt{i_c}$, a linear relationship is not obtained, as shown in Figure 2. However, the $\vec{\alpha}$ value can be iteratively increased until the required linear relationship is obtained between the charging function and $\sqrt{i_c}$, as shown by the data for $\vec{\alpha}' = 0.30$ in Figure 2.

Figures 3a and b show the charging function vs. $\sqrt{i_c}$ for iron and nickel electrodes at several pH values. As indicated in Table 1, the correlation coefficients (R^2) for the best-fit $\vec{\alpha}$ values generally decreased with decreasing

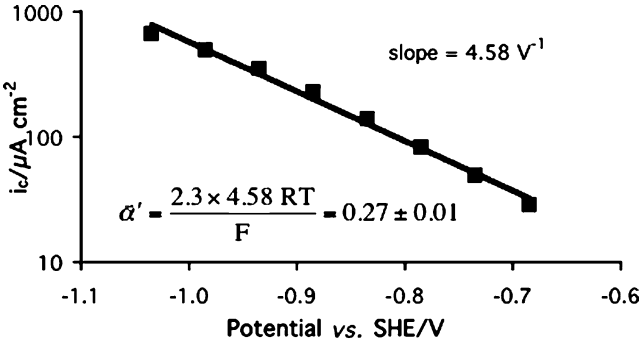

Fig. 1. Steady state currents as a function of the applied potential for an iron rotating disk electrode in a 10 mM $CaSO_4$ solution at a pH value of 7.

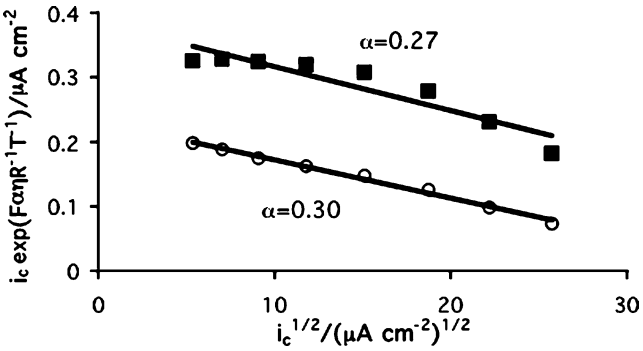

Fig. 2. Charging function vs. $\sqrt{i_c}$ for the data in Figure 1 for two different electron transfer coefficient values.

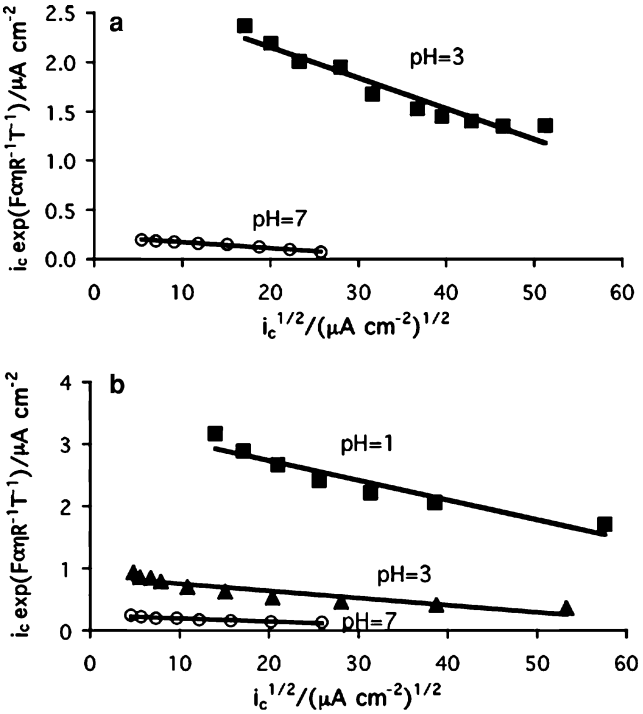

Fig. 3. Charging function vs. $\sqrt{i_c}$ at different pH values using the best-fit $\vec{\alpha}$ values listed in Table 1 for iron [a] and nickel [b] rotating disk electrodes.

Table 1. Best-fit electron transfer coefficients [$\vec{\alpha}$] and their corresponding correlation coefficients [R^2] along with exchange current densities [i_0] and discharge [k_1] and recombination [k_2] rate constants for iron and nickel electrodes in $CaSO_4$ electrolyte solutions at different pH values

Electrode	pH	$\vec{\alpha}$	R^2	i_0 (μA cm^{-2})	k_1 (cm s^{-1})	k_2 (μmol cm^{-2} s^{-1})
Iron	7	0.30	0.99	0.23	6.7×10^{-3}	1.5×10^{-2}
Iron	3	0.50	0.93	2.7	7.7×10^{-6}	8.9×10^{-2}
Nickel	7	0.30	0.88	0.25	7.1×10^{-3}	2.5×10^{-2}
Nickel	3	0.39	0.91	0.76	2.2×10^{-6}	5.9×10^{-2}
Nickel	1	0.50	0.85	3.4	9.8×10^{-8}	1.1×10^{-1}

pH value. This can likely be attributed to an increasing contribution of reaction 3 to the HER with decreasing pH values. For both the iron and nickel electrodes, the best-fit $\vec{\alpha}$ values were found to decrease with decreasing pH values, as shown in Table 1. According to the proposed HER mechanism with reaction 1 as the rate-limiting step, $\vec{\alpha}$ should not be a function of the solution pH value. This apparent contradiction can be explained by the presence of oxide functional groups on the electrode surfaces that may specifically adsorb protons or other ions in the solution (e.g., SO_4^{2-}). Specific adsorption of ions at the electrode surface will be both pH and potential dependent, and will affect the apparent electron transfer coefficient through its impact on the electrical double layer [37].

At pH values sufficiently low to dissolve oxides coating the electrode surfaces, $\vec{\alpha}$ values of 0.50 were obtained for both the iron and nickel electrodes, as shown in Table 1. These values are close to those previously reported for the HER on iron, nickel and other metal electrodes in acid solutions [27]. The fact that a lower pH value was required for the nickel electrode to achieve $\vec{\alpha} = 0.5$ is consistent with the greater difficulty in dissolving nickel, as compared to iron, oxides [38]. Previous research has found that the β-$Ni[OH]_2$ that forms on nickel cathodes is resistant to both reduction and dissolution [39].

Once the best-fit $\vec{\alpha}$ values have been iteratively determined, the slope and intercept of the linear profiles in Figure 3 can be used to determine k_2 and i'_0 values. For each potential where i_c was measured, θ_H can then be determined from equation 7. Figure 4 shows θ_H values calculated for iron and nickel electrodes at several pH values. The rate constants and exchange currents calculated from the data in Figure 3 are summarized in Table 1. At a pH value of 3, the exchange current

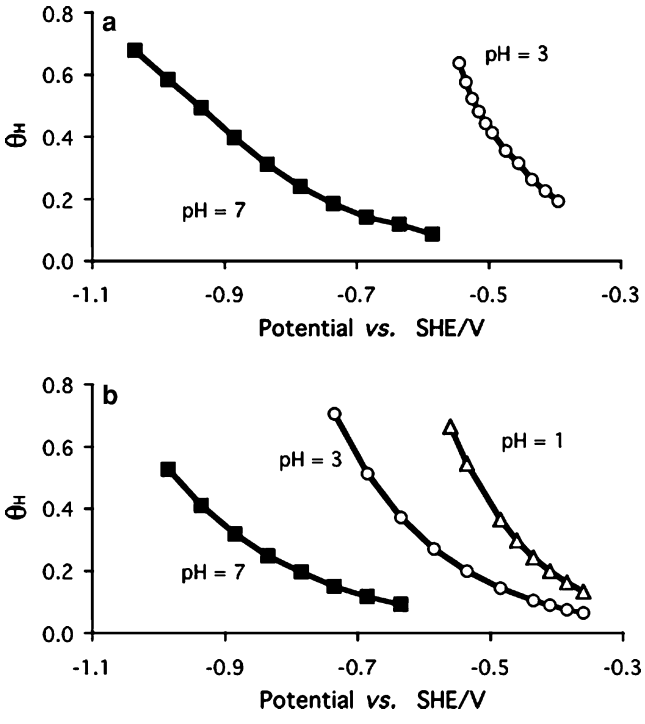

Fig. 4. Fractional hydrogen surface coverages [θ_H] as a function of electrode potential at different pH values for iron [a] and nickel [b] rotating disk electrodes.

Table 2. Corrosion current densities [i_{corr}] and fractional hydrogen surface coverages [θ_H^{ocp}] under open circuit conditions for iron and nickel electrodes at different pH values in $CaSO_4$ electrolyte solutions

Electrode material	pH	i_{corr} (μA cm^{-2})	θ_H^{ocp}	E_{corr} vs. SHE (mV)
Iron	7	0.73	0.022	−0.547
Iron	3	32	0.061	−0.335
Nickel	7	0.64	0.016	−0.536
Nickel	3	28	0.070	−0.349
Nickel	1	63	0.076	−0.312

density for the iron electrode of 2.7 μA cm^{-2} is close to the value of 2.0 μA cm^{-2} that has been previously reported for iron at a pH value of 1 [30]. For the nickel electrode at a pH value of 1, the exchange current density of 3.4 μA cm^{-2} is within a factor of two of the value of 6.3 μA cm^{-2} that has been previously reported for nickel in acid solutions [27].

Because the free corrosion potentials for iron and nickel electrodes are significantly below the E_{eq} for the HER reaction, the rate of atomic hydrogen oxidation on the electrode surface will be small compared to the rate of H^+ reduction. Therefore, corrosion current densities (i_{corr}) determined from Tafel scans and k_2 values determined from the polarization experiments can be used to determine θ_H^{ocp} values. Under open circuit conditions, i_c is equivalent to i_{corr}, and the hydrogen surface coverage can be determined from:

$$\theta_H^{ocp} = \frac{\sqrt{i_{corr}}}{\sqrt{Fk_2}} \tag{9}$$

As shown in Table 2, i_{corr} values for the iron and nickel electrodes at several pH values ranged from 0.73 to 63 μA. From the k_2 values in Table 1, θ_H^{ocp} values ranging from 0.016 to 0.076 were obtained for the iron and nickel electrodes.

5. Conclusions

This research investigated a method for determining θ_H values for oxide-coated iron and nickel surfaces under conditions where the electron transfer coefficients may deviate significantly from 0.5. The method is valid at neutral and alkaline pH values where the Volmer discharge reaction is the rate-limiting step for hydrogen evolution. Determination of the effects of electrode potential and solution pH values on adsorbed concentrations of atomic hydrogen may aid in elucidating reaction mechanisms responsible for reductive dechlorination of solvents in contaminated waters.

Acknowledgements

This project was made possible by Grant No. 2P42ES04940-11 from the National Institutes for Environmental Health Sciences of the National Institutes for Health, with funds from the U.S. Environmental Protection Agency.

References

1. S. Tamilmani, W.H. Huang, S. Raghavan and J. Farrell, *IEEE Trans. Semicond. Manuf.* **17** (2004) 448.
2. J.N. Fiedor, W.D. Bostick, R.J. Jarabek and J. Farrell, *Environ. Sci. Technol.* **32** (1998) 1466.
3. J. Farrell, W.D. Bostick, J.N. Fiedor and R.J. Jarabek, *Environ. Sci. Technol.* **33** (1999) 1244.
4. J.P. Gould, *Water Res.* **16** (1982) 871.
5. R.M. Powell, R.W. Puls, S.K. Hightower and D.A. Sabatini, *Environ. Sci. Technol.* **29** (1995) 1913.
6. D.P. Siantar, C.G. Schrier, C.S. Chou and M. Reinhard, *Water Res.* **30** (1996) 2315.
7. Y.H. Huang, T.C. Zhang, P.J. Shea and S.D. Comfort, *J. Environ. Qual.* **32** (2003) 1306.
8. N. Melitas, O. Chuffe and J. Farrell, *Environ. Sci. Technol.* **35** (2001) 3948.
9. R.W. Gillham and S.F. O'Hannesin, *Ground Water* **32** (1994) 958.
10. L.J. Matheson and P.G. Tratnyek, *Environ. Sci. Technol.* **28** (1994) 2045.
11. A.G. Vlyssides, M. Loizidou, P.K. Karlis and A.A. Zorpas, *Hazard. Ind. Wastes* **31** (1999) 147.
12. S. Nam and P.G. Tratnyek, *Water Res.* **34** (2000) 1837.
13. W. Zhang and B. Chuan, Rapid and Complete Dechlorination of TCE and PCB's by Nanoscale Fe and Pd/Fe Particles. Abstracts of the 213th Meeting of the American Chemical Society, San Francisco, 13–17 April (1997) 37, pp. 78–79.
14. F. Murena and E. Schioppa, *Appl. Catal. B* **27** (2000) 257.
15. J.D. Rodgers and N.J. Bunce, *Environ. Sci. Technol.* **35** (2001) 406.
16. A. Agrawal and P.G. Tratnyek, *Environ. Sci. Technol.* **30** (1996) 153.
17. Z. Liu, R.G. Arnold, E.A. Betterton and K.D. Festa, *Env. Eng. Sci.* **16** (1999) 1.
18. M.C. Helvenston, R.W. Presley and B. Zhao, Electro-reductive Dehalogenation on Palladized Graphite Electrodes. Abstracts of the 213th Meeting of the American Chemical Society, San Francisco, 13–17 April (1997) 37, pp. 294–297.
19. F.L. Lambert, B.L. Hasslinger and R.N. Franz, *J. Electrochem. Soc.* **122** (1975) 737.
20. W.A. Arnold and A.L. Roberts, *Environ. Sci. Technol.* **32** (1998) 3017.
21. C. Su and R.W. Puls, *Environ. Sci. Technol.* **33** (1999) 163.
22. T. Boronina, K.J. Klabunde and G. Sergeev, *Environ. Sci. Technol.* **29** (1995) 1511.
23. J. Wang and J. Farrell, *Environ. Sci. Technol.* **37** (2003) 3891.
24. T. Li and J. Farrell, *Environ. Sci. Technol.* **34** (2000) 173.
25. I.M. Koltoff, T.S. Lee, D. Stocesova and E.P. Parry, *Anal. Chem.* **22** (1950) 521.
26. J. Wang, P. Blowers and J. Farrell, *Environ. Sci. Technol.* **38** (2004) 1576.
27. J.O'M. Bockris and A.K. Reddy, *Modern Electrochemistry, Volume 2* (Plenum Press, New York, 1970).
28. J.O'M. Bockris, J.L. Carbajal, B.R. Scharifker and K. Chandrasekaran, *J. Electrochem. Soc.* **134** (1987) 1957.
29. H.J. Flitt and J.O'M. Bockris, *Int. J. Hydrogen Energy* **7** (1982) 411.
30. M.H. Abd Elhamid, B.G. Ateya, K.G. Weil and H.W. Pickering, *J. Electrochem. Soc.* **147** (2000) 2148.
31. T.M. Sivavec, P.D. Mackenzie, D.P. Horney and S.S. Baghel, in Proceedings of the International Containment Technology Conference, St. Petersburg, FL, 9–12 Feb. (1997) pp. 753–759.
32. L. Gui, R.W. Gillham and M.S. Odziemkowski, *Environ. Sci. Technol.* **34** (2000) 3489.

33. A.J. Bard and L.R. Faulkner, *Electrochemical Methods* (John Wiley and Sons, New York, 1980).
34. J.O'M. Bockris and E.C. Potter, *J. Chem. Phys.* **20** (1952) 614.
35. T. Li and J. Farrell, *Environ. Sci. Technol.* **35** (2001) 3560.
36. H.S. Fogler, *Elements of Chemical Reaction Engineering*, 3rd ed., (Prentice-Hall, Upper Saddle River, NJ, 1999).
37. G. Pezzatini and R. Guidelli, *J. Electroanal. Chem.* **76** (1977) 51.
38. J.W. Kim and S.T. Park, *J. Electrochem. Soc.* **146** (1999) 1075.
39. P.A. Christensen and A. Hamnet, *Techniques and Mechanisms in Electrochemistry* (Chapman and Hall, Oxford, 1994).